Journal of Quantitative Spectroscopy & Radiative Transfer 326 (2024) 109102

Contents lists available at ScienceDirect

Journal of Quantitative Spectroscopy and Radiative Transfer

journal homepage: www.elsevier.com/locate/jqsrt

View factor of a spheroid and an ellipse from a plate element

Kaname Sasaki

German Space Center (DLR), Institute of Space Systems, Robert-Hooke-Str. 7, 28359, Bremen, Germany

ARTICLE INFO

Keywords:
View factor
Radiative heat transfer
Spheroid
Ellipse

ABSTRACT

A view factor is a fundamental parameter for evaluating radiative heat transfer between two surfaces. View factors for various geometries have been investigated in the past studies. However, the view factors of a spheroid and an ellipse are known only for limited configurations. In this study, the analytical view factor expressions of an ellipse and a spheroid from a plate element are derived. The spheroid view factor solution applies to a plate element with any position and orientation, and the ellipse solution is valid when the plate element is on the perpendicular axis through the ellipse center. The derived analytical solutions are validated against the numerical results for various configurations, showing deviations of less than 0.0001 for all cases.

1. Introduction

For evaluating radiative heat transfer between two surfaces, one of the difficulties is to specify how much energy leaves one surface and arrives at the other surface. Under the assumption of the diffuse surfaces, a view factor is the geometric parameter that characterizes this process. View factors for various types of geometries have been investigated in the past studies, and Howell and Mengüç compiled the collection of analytical view factor solutions [1,2].

Analytical view factor expressions for sphere-related geometries exist for various configurations. Investigations on the sphere view factors from standard geometries, such as a plate element, a disk, a rectangle, a sphere and a cylinder, can be found in the series of studies performed by Chung, Naraghi, and Sabet [3–5]. Also, the view factor of a part of a sphere from the plate element has been investigated in the past [6,7]. In the study of Naraghi and Chung [4,8], the view factors of various types of axi-symmetric body from a disk and a sphere were examined. For spheroids, the view factor is partially expressed in the analytical form, but the other part contains unsolved integral terms. Cabeza-Lainez and Pulido-Arcas studied the view factor between the internal surface of a spheroid and a disk, considering the reciprocal relation of the view factor [9]. However, for the external surface of a spheroid, the analytical expression is not available.

The view factor of a spheroid is expected to be useful as the generalization of the sphere view factor. One of the possible application areas of the spheroid view factor is the thermal radiation hazard assessment from industrial fires, such as fireballs and jet flames. In the study of Blankenhagel et al. [10], the fireball shape is observed using infrared cameras, and the equivalent sphere diameter is evaluated based on volume. In this way, the fireball shape is simplified as a sphere and the radiative heat flux from the fireball is estimated based on the sphere view factor. For the evaluation of the jet fire, the shape of the flame is often modeled by a cylinder, a cone, a spheroid, and combination of these shapes [11–15]. Also, in the study of flame under microgravity, the ellipsoidal shape is considered for modeling the flame [16], and for evaluating the experimental test results [17,18].

Another application can be found in the thermal radiation modeling of plants. In the study of Colaizzi et al. [19,20], crop rows are modeled as elliptical hedgerows, and the view factor of the crop canopy from above is used to evaluate the radiation reflected from the vegetated surface. Similarly, in the study by Zhang et al. [21], tree canopies are modeled as the spheroidal shapes to numerically evaluate the radiative heat exchange between the trees and the adjacent wall.

In the field of aerospace engineering, one application example is the radiative heat transfer analysis of aerostats [22,23]. In these studies, the aerostat is modeled as a spheroid, and the view factor between the aerostat surface and the ground is numerically evaluated. Other application possibilities can be found in the thermal analysis for space missions. For the thermophysical modeling of the smaller body in the 65803 Didymos system, the geometry is modeled as a ellipsoid and the radiative heat exchange with the primary body is numerically evaluated by using the view factor [24]. Also, for the general spacecraft thermal modeling, spheroidal and ellipsoidal surface is used to construct the spacecraft geometry and perform numerical analysis [25].

In this study, the analytical formulas of the spheroid view factor from a plate element are studied. As the projected shape of a spheroid is an ellipse, the ellipse view factor from a plate element is derived first. Subsequently, the spheroid view factor is derived by using the ellipse view factor with necessary parameter transformations.

E-mail address: kaname.sasaki@dlr.de.

https://doi.org/10.1016/j.jqsrt.2024.109102
Received 24 May 2024; Accepted 23 June 2024
Available online 29 June 2024

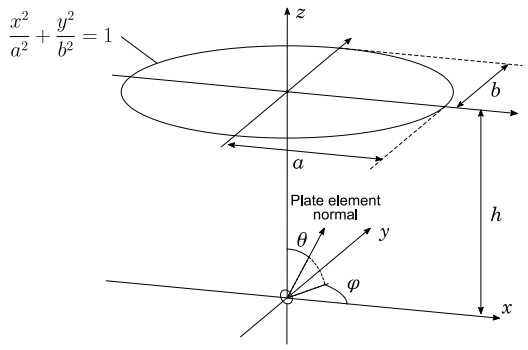

Fig. 1. Ellipse view factor from a plate element.

2. View factor of an ellipse

Before deriving the analytical view factor of a spheroid, we first discuss the ellipse view factor from a plate element. For a circular disk, the view factor from the differential surface is known for general position and orientation [26,27]. However, for an ellipse, the analytical expression is available only for special cases [28,29]. Considering the later application for calculating the spheroid view factor, the discussion focuses on ellipse view factor from a plate element, which is placed on the normal line passing through the ellipse center.

Fig. 1 illustrates the configuration of the ellipse and the plate element. We assume that the plate element is located at the origin with an arbitrary orientation, and the ellipse is expressed as

$$\frac{x^2}{a^2}+\frac{y^2}{b^2}=1, \quad \text{and} \quad z=h. \tag{1}$$

where a and b are the semi-major and semi-minor axes, respectively. The orientation of the plate element (l,m,n) is described by using the angular parameters θ and φ.

$$\begin{bmatrix} l \\ m \\ n \end{bmatrix} = \begin{bmatrix} \sin\theta\cos\varphi \\ \sin\theta\sin\varphi \\ \cos\theta \end{bmatrix}. \tag{2}$$

The extended surface of the plate element is given by

$$x\sin\theta\cos\varphi + y\sin\theta\sin\varphi + z\cos\theta = 0. \tag{3}$$

The intersection of this surface with $z=h$ is described as a line on $z=h$ surface.

$$y = -\frac{\cos\varphi}{\sin\varphi}x - \frac{h\cos\theta}{\sin\theta\sin\varphi}. \tag{4}$$

Substituting Eq. (4) into the ellipse equation Eq. (1), we obtain

$$\frac{x^2}{a^2}+\frac{1}{b^2}\left(\frac{\cos\varphi}{\sin\varphi}x+\frac{h\cos\theta}{\sin\theta\sin\varphi}\right)^2 = 1. \tag{5}$$

The discriminant of the quadratic equation Eq. (5) shall be zero, when the line is tangent to the ellipse. From this condition, the extended surface of the plate element is tangent to the ellipse when the following equation is satisfied.

$$\tan^2\theta = \frac{h^2}{b^2\sin^2\varphi + a^2\cos^2\varphi}. \tag{6}$$

Thus, depending on the value of θ, the visibility of the ellipse from the plate element is classified into three cases.

$$\text{Case 1, complete ellipse}: 0 \le \theta \le \theta_{\tan}, \tag{7}$$

$$\text{Case 2, partial ellipse}: \theta_{\tan} < \theta < \pi - \theta_{\tan}, \tag{8}$$

$$\text{Case 3, no ellipse}: \pi - \theta_{\tan} \le \theta \le \pi, \tag{9}$$

$$\text{where} \quad \theta_{\tan} = \arctan\frac{h}{\sqrt{b^2\sin^2\varphi + a^2\cos^2\varphi}}. \tag{10}$$

In general, the view factor can be calculated by using the contour integral [30]. For calculating the ellipse view factor from a plate element, the contour integral is performed around the visible part of the ellipse.

$$F_{\text{ellipse}} = l\int\frac{z\,dy - y\,dz}{2\pi S^2} + m\int\frac{x\,dz - z\,dx}{2\pi S^2} + n\int\frac{y\,dx - x\,dy}{2\pi S^2}, \tag{11}$$

where S is the distance between the plate element and the integration line. For cases where the complete ellipse is visible, the line integration shall be performed along the complete ellipse edge. On the other hand, when the ellipse is partially visible, the line integration shall be performed partially along the ellipse edge, and along the intersection line of the ellipse surface and the extended surface of the plate element.

2.1. Case 1: complete ellipse

By using the angular parameter α, the edge of the ellipse can be described by

$$\begin{bmatrix} x \\ y \\ z \end{bmatrix} = \begin{bmatrix} a\cos\alpha \\ b\sin\alpha \\ h \end{bmatrix}. \tag{12}$$

$$\frac{d}{d\alpha}\begin{bmatrix} x \\ y \\ z \end{bmatrix} = \begin{bmatrix} -a\sin\alpha \\ b\cos\alpha \\ 0 \end{bmatrix}. \tag{13}$$

The distance between the plate element and the ellipse arc is described by

$$S^2 = a^2\cos^2\alpha + b^2\sin^2\alpha + h^2. \tag{14}$$

By substituting the parametric ellipse equations Eqs. (12)–(14) to the view factor equation Eq. (11), the line integration formula along the ellipse arc can be obtained.

$$\begin{aligned} L_{\text{arc}} =& \frac{lhb}{2\pi(a^2+h^2)}\int\frac{\cos\alpha\,d\alpha}{1-\frac{a^2-b^2}{a^2+h^2}\sin^2\alpha} \\ &+ \frac{mha}{2\pi(a^2+h^2)}\int\frac{\sin\alpha\,d\alpha}{1-\frac{a^2-b^2}{a^2+h^2}\sin^2\alpha} \\ &- \frac{nab}{2\pi(a^2+h^2)}\int\frac{d\alpha}{1-\frac{a^2-b^2}{a^2+h^2}\sin^2\alpha}. \end{aligned} \tag{15}$$

Assuming $a > b$, each integration can be performed analytically. Executing this integration from α_0 to α_1, the analytical result is given by

$$\begin{aligned} L_{\text{arc}} =& \frac{lhb}{2\pi(a^2+h^2)}\left[\frac{\tanh^{-1}(c\sin\alpha)}{c}\right]_{\alpha_0}^{\alpha_1} + \frac{mha}{2\pi(a^2+h^2)} \\ &\times\left[-\frac{1}{c\sqrt{1-c^2}}\left\{\arctan\left(\frac{c-\tan\frac{\alpha}{2}}{\sqrt{1-c^2}}\right)+\arctan\left(\frac{c+\tan\frac{\alpha}{2}}{\sqrt{1-c^2}}\right)\right\}\right]_{\alpha_0}^{\alpha_1} \\ &- \frac{nab}{2\pi(a^2+h^2)}\left[\frac{\arctan(\sqrt{1-c^2}\tan\alpha)}{\sqrt{1-c^2}}\right]_{\alpha_0}^{\alpha_1}, \end{aligned} \tag{16}$$

$$\text{where} \quad c = \sqrt{\frac{a^2-b^2}{a^2+h^2}}. \tag{17}$$

When the complete ellipse is visible from the plate element, the line integration shall be performed along the complete ellipse edge, for example $\alpha_0 = \pi$, $\alpha_1 = -\pi$. In this case, the view factor is expressed in the simple analytical form.

$$F_{\text{complete ellipse}} = \frac{ab\cos\theta}{\sqrt{(a^2+h^2)(b^2+h^2)}}. \tag{18}$$

This results is consistent with the result for $\theta = 0$ case, which is presented in the past literatures [28,29].

2.2. Case 2: partial ellipse

When the ellipse is partially visible from the plate element, the integration along the intersection line is required as well. The two intersection points between the ellipse edge and the extended plate element are specified by solving the following three equations.

$$z = h, \tag{19}$$

$$\frac{x^2}{a^2} + \frac{y^2}{b^2} = 1, \tag{20}$$

$$x \sin\theta \cos\varphi + y \sin\theta \sin\varphi + z \cos\theta = 0. \tag{21}$$

For $\varphi = 0$ or $\varphi = \frac{\pi}{2}$, the intersection points are

$$\varphi = 0 : \ x = -\frac{h\cos\theta}{\sin\theta}, \quad y = \pm\frac{b}{a}\sqrt{a^2 - x^2}, \tag{22}$$

$$\varphi = \frac{\pi}{2} : \ y = -\frac{h\cos\theta}{\sin\theta}, \quad x = \pm\frac{a}{b}\sqrt{b^2 - y^2}. \tag{23}$$

For the other cases, the intersection points are calculated as

$$y = -\frac{\cos\varphi}{\sin\varphi}x - \frac{h\cos\theta}{\sin\theta\sin\varphi}, \tag{24}$$

$$x = \frac{-B \pm \sqrt{B^2 - AC}}{A}, \tag{25}$$

$$\text{where} \begin{cases} A = \frac{1}{a^2} + \frac{\cos^2\varphi}{b^2\sin^2\varphi}, \\ B = \frac{h}{b^2}\frac{\cos\theta\cos\varphi}{\sin\theta\sin^2\varphi}, \\ C = \frac{h^2\cos^2\theta}{\sin^2\theta\sin^2\varphi} - 1. \end{cases} \tag{26}$$

In the following discussion, the acquired two intersection points are denoted as (x_0, y_0, h) and (x_1, y_1, h), where $x_0 \le x_1$. The corresponding angular parameters are specified by

$$\alpha_0 = \arctan(ay_0, bx_0), \tag{27}$$

$$\alpha_1 = \arctan(ay_1, bx_1). \tag{28}$$

Now, the line from (x_1, y_1, h) to (x_0, y_0, h) is expressed as

$$\begin{bmatrix} x \\ y \\ z \end{bmatrix} = \beta \begin{bmatrix} x_0 - x_1 \\ y_0 - y_1 \\ 0 \end{bmatrix} + \begin{bmatrix} x_1 \\ y_1 \\ h \end{bmatrix}, \tag{29}$$

$$\frac{d}{d\beta}\begin{bmatrix} x \\ y \\ z \end{bmatrix} = \begin{bmatrix} x_0 - x_1 \\ y_0 - y_1 \\ 0 \end{bmatrix}. \tag{30}$$

In this case, the distance between the plate element and the integration line is described by

$$S^2 = \{\beta(x_0 - x_1) + x_1\}^2 + \{\beta(y_0 - y_1) + y_1\}^2 + h^2 \tag{31}$$

By substituting Eqs. (29)–(31) to the view factor equation Eq. (11), the line integration formula along the intersection line can be obtained.

$$L_{\text{intersect}} = \frac{1}{2\pi}\int_0^1 \frac{N\, d\beta}{K\beta^2 + 2L\beta + M}, \tag{32}$$

where

$$K = (x_0 - x_1)^2 + (y_0 - y_1)^2, \tag{33}$$

$$L = (x_0 - x_1)x_1 + (y_0 - y_1)y_1, \tag{34}$$

$$M = x_1^2 + y_1^2 + h^2, \tag{35}$$

$$N = lh(y_0 - y_1) - mh(x_0 - x_1) + n(y_1x_0 - x_1y_0). \tag{36}$$

The solution of this integral is obtained as the following analytical form.

$$L_{\text{intersect}} = \frac{N}{2\pi\sqrt{-L^2 + KM}}\left\{\arctan\left(\frac{K + L}{\sqrt{-L^2 + KM}}\right) - \arctan\left(\frac{L}{\sqrt{-L^2 + KM}}\right)\right\}. \tag{37}$$

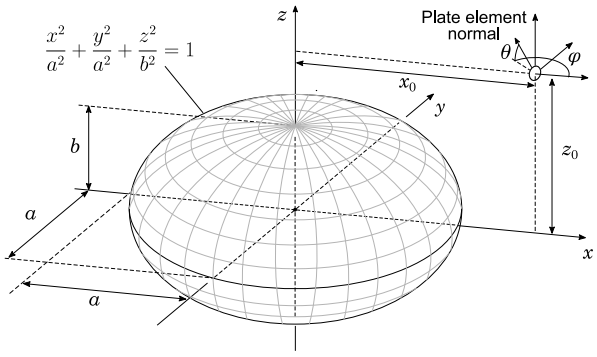

Fig. 2. Spheroid view factor from a plate element.

Therefore, the view factor of the partially visible ellipse is calculated by

$$F_{\text{partial ellipse}} = L_{\text{arc}} + L_{\text{intersect}}. \tag{38}$$

3. View factor of a spheroid

In this section, we derive the analytical expression of the spheroid view factor from a plate element. Instead of performing the area or line integration on the spheroid surface, the projected shape of the spheroid is investigated, in order to specify the equivalent solution as the ellipse view factor.

The configuration of the spheroid and the plate element is illustrated in Fig. 2. The corresponding spheroid equation is

$$\frac{x^2}{a^2} + \frac{y^2}{a^2} + \frac{z^2}{b^2} = 1, \tag{39}$$

where a and b are the equatorial radius and the distance from the center to the pole, respectively. Considering the axi-symmetric shape of the spheroid, it is possible to assume that the position of the differential surface is located in the positive part of the xz-plane. The coordinates of the plate element are expressed as $(x_0,\ 0,\ z_0)$, where $x_0 \ge 0$ and $z_0 \ge 0$. The normal vector of the plate element is described by $(\cos\theta\cos\varphi,\ \cos\theta\sin\varphi,\ \sin\theta)$. While Fig. 2 depicts an oblate spheroid, the following discussion is also applicable to a prolate spheroid.

For calculating the view factor from the plate element, evaluating the projected shape on a screen is equivalent to evaluate the original object. In general cases, it requires complex calculation to specify the exact image of the spheroid on the screen, as discussed in [31,32]. In this study, we pre-define the screen orientation and the new coordinates, so that the projected shape forms an ellipse, where the axes of the ellipse are aligned with the coordinate axes.

The initial configuration of the spheroid, plate element, and screen is illustrated in Fig. 3(a). Considering the symmetry of the spheroid, the screen orientation is defined by one angular parameter γ_0. Since it does not influence the resulting view factor value, the distance between the plate element and the screen is set to unity. As the next step, we shift the coordinate origin to the plate element and rotate the coordinate system around the y-axis by $-\gamma_0$ as shown in Fig. 3(b). This coordinate system is specified by $X_sY_sZ_s$-axes, and the image of the spheroid on the screen should be presented as the function of Y_s and Z_s. In order to specify Y_s as the function of γ, we consider the intersection of the spheroid and a surface, which is inclined by γ with regard to the X_sY_s-plane. In Fig. 3(c), the inclined surface is coincide with the XY-plane by rotating the coordinate system around the y-axis additionally by $-\gamma$. In this coordinate system, the spheroid is described by

$$\frac{\{\cos(\gamma_0 + \gamma)X - \sin(\gamma_0 + \gamma)Z + x_0\}^2}{a^2} + \frac{Y^2}{a^2} + \frac{\{\sin(\gamma_0 + \gamma)X - \cos(\gamma_0 + \gamma)Z + z_0\}^2}{b^2} = 1. \tag{40}$$

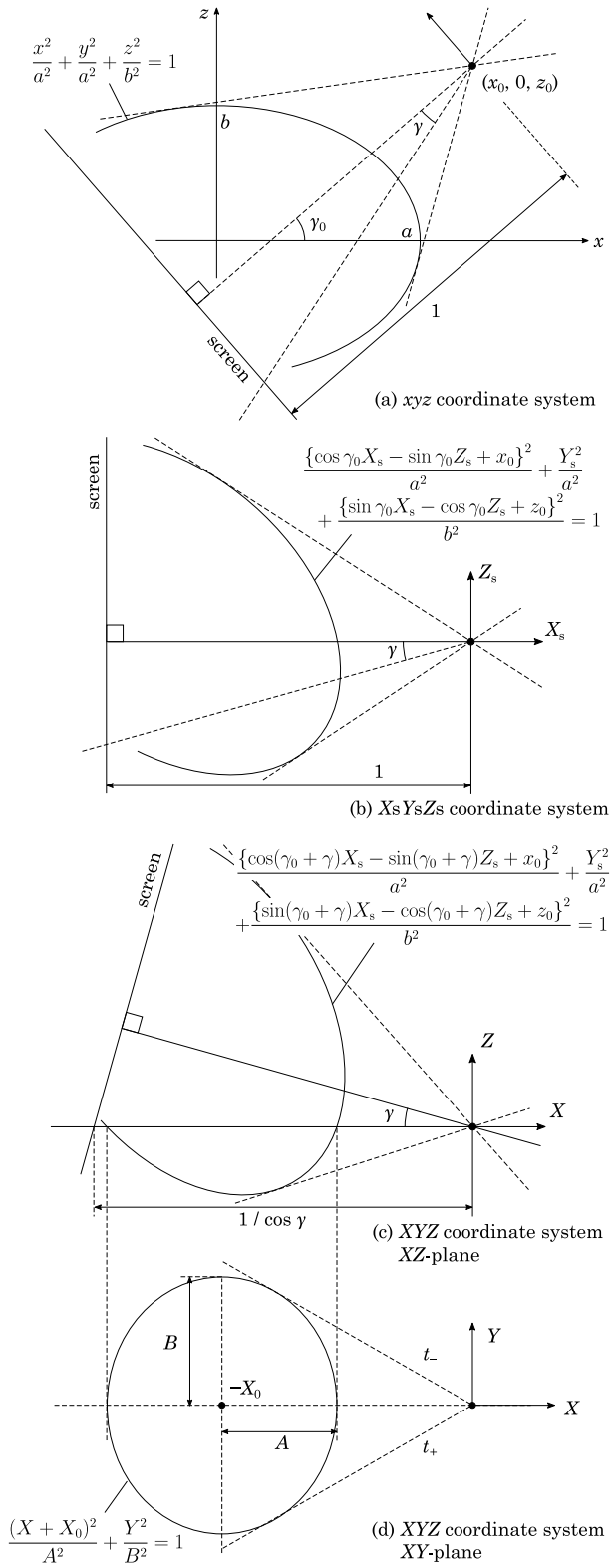

Fig. 3. Spheroid and a plate element in different coordinate systems.

The intersection of the spheroid and the XY-plane is specified by Eq. (41), and geometrically shown in Fig. 3(d).

$$\frac{(X+X_0)^2}{A}+\frac{Y^2}{B}=1, \tag{41}$$

where

$$X_0=\frac{b^2x_0\cos(\gamma_0+\gamma)+a^2z_0\sin(\gamma_0+\gamma)}{b^2\cos^2(\gamma_0+\gamma)+a^2\sin^2(\gamma_0+\gamma)}, \tag{42}$$

$$A=\frac{a^2b^2-b^2x_0^2-a^2z_0^2}{b^2\cos^2(\gamma_0+\gamma)+a^2\sin^2(\gamma_0+\gamma)}+X_0^2, \tag{43}$$

$$B=\left\{\cos^2(\gamma_0+\gamma)+\frac{a^2}{b^2}\sin^2(\gamma_0+\gamma)\right\}A. \tag{44}$$

When $A>0$, Eq. (41) represents an ellipse. The tangential lines from the coordinate origin to the ellipse on the XY-plane are given by

$$Y=t_\pm X,\quad \text{where}\quad t_\pm=\pm\sqrt{\frac{B}{X_0^2-A}}. \tag{45}$$

Based on this result, the coordinates of the image outline on the screen are described by

$$Y_s=\frac{1}{\cos\gamma}\sqrt{\frac{B}{X_0^2-A}}, \tag{46}$$

$$-Z_s=\tan\gamma. \tag{47}$$

The relation of Y_s and Z_s can be presented in the following form.

$$Y_s^2=A_sZ_s^2+B_sZ_s+C_s, \tag{48}$$

where

$$\begin{aligned}A_s=\frac{1}{b^2}\Bigg\{&-b^2\sin^2\gamma_0-a^2\cos^2\gamma_0\\&+\frac{b^4x_0^2\sin^2\gamma_0}{-a^2b^2+b^2x_0^2+a^2z_0^2}-\frac{2a^2b^2x_0z_0\cos\gamma_0\sin\gamma_0}{-a^2b^2+b^2x_0^2+a^2z_0^2}\\&+\frac{a^4z_0^2\cos^2\gamma_0}{-a^2b^2+b^2x_0^2+a^2z_0^2}\Bigg\},\end{aligned} \tag{49}$$

$$\begin{aligned}B_s=\frac{1}{b^2}\Bigg\{&-2b^2\cos\gamma_0\sin\gamma_0+2a^2\cos\gamma_0\sin\gamma_0\\&+\frac{2b^4x_0^2\cos\gamma_0\sin\gamma_0}{-a^2b^2+b^2x_0^2+a^2z_0^2}-\frac{2a^2b^2x_0z_0(\cos^2\gamma_0-\sin^2\gamma_0)}{-a^2b^2+b^2x_0^2+a^2z_0^2}\\&-\frac{2a^4z_0^2\cos\gamma_0\sin\gamma_0}{-a^2b^2+b^2x_0^2+a^2z_0^2}\Bigg\},\end{aligned} \tag{50}$$

$$\begin{aligned}C_s=\frac{1}{b^2}\Bigg\{&-b^2\cos^2\gamma_0-a^2\sin^2\gamma_0\\&+\frac{b^4x_0^2\cos^2\gamma_0}{-a^2b^2+b^2x_0^2+a^2z_0^2}+\frac{2a^2b^2x_0z_0\cos\gamma_0\sin\gamma_0}{-a^2b^2+b^2x_0^2+a^2z_0^2}\\&+\frac{a^4z_0^2\sin^2\gamma_0}{-a^2b^2+b^2x_0^2+a^2z_0^2}\Bigg\}.\end{aligned} \tag{51}$$

Eq. (48) suggests that the possible image on the screen is outlined by a quadratic curve. The equation can be re-written in the following form.

$$\frac{Y_s^2}{C_s-\frac{B_s^2}{4A_s}}-\frac{\left(Z_s-\frac{B_s^2}{2A_s}\right)^2}{\frac{1}{A_s}\left(C_s-\frac{B_s^2}{4A_s}\right)}=1. \tag{52}$$

When the following two conditions are satisfied, the image exists on the screen as an ellipse.

$$A_s<0, \tag{53}$$

$$B_s^2-4A_sC_s>0. \tag{54}$$

Substituting Eqs. (49)–(51) into Eq. (54), the condition can be concretely presented as shown in Eq. (55), and it is confirmed that the condition is satisfied when the plate element is placed outside of the

spheroid.

$$B_s^2 - 4A_sC_s = \frac{4a^4}{-a^2b^2 + b^2x_0^2 + a^2z_0^2} > 0. \tag{55}$$

The condition of Eq. (53) specifies the range of γ_0. Depending on the value of $b - z_0$, the range of γ_0 is described by the following forms.

(a) $b - z_0 > 0$:

$$\tan\gamma_0 > \frac{+x_0z_0 - \sqrt{-a^2b^2 + a^2x_0^2 + b^2x_0^2}}{b^2 - z_0^2}, \quad \text{and}$$

$$\tan\gamma_0 < \frac{+x_0z_0 + \sqrt{-a^2b^2 + a^2x_0^2 + b^2x_0^2}}{b^2 - z_0^2}. \tag{56}$$

(b) $b - z_0 = 0$: $\quad \tan\gamma_0 > \dfrac{a^2 - x_0^2}{2x_0z_0}.$ (57)

(c) $b - z_0 < 0$:

$$\tan\gamma_0 < \frac{-x_0z_0 - \sqrt{-a^2b^2 + a^2x_0^2 + b^2x_0^2}}{-b^2 + z_0^2}, \quad \text{or}$$

$$\tan\gamma_0 > \frac{-x_0z_0 + \sqrt{-a^2b^2 + a^2x_0^2 + b^2x_0^2}}{-b^2 + z_0^2}. \tag{58}$$

Meanwhile, we require $B_s = 0$, so that the image is symmetric with respect to the $Z_s = 0$ plane. This condition specifies the parameter γ_0 as shown in Eqs. (59)–(60).

$$\tan 2\gamma_0 = \frac{2x_0z_0}{a^2 - x_0^2 - b^2 + z_0^2}, \tag{59}$$

$$\tan\gamma_0 = -\frac{1}{\tan 2\gamma_0} \pm \sqrt{\frac{1}{\tan^2 2\gamma_0} + 1}. \tag{60}$$

Geometrically, γ_0 corresponds to the middle line of the range specified by Eqs. (56)–(58), and so the value with a positive sign in Eq. (60) has to be selected. For the special cases, where $x_0 = 0$ or $z_0 = 0$, the value of γ_0 is determined as shown in Eqs. (61)–(62).

$$z_0 = 0 : \quad \gamma_0 = 0, \tag{61}$$

$$x_0 = 0 : \quad \gamma_0 = \frac{\pi}{2}. \tag{62}$$

Using the specified γ_0, the image exists on the screen as an ellipse, with the ellipse axes aligned to the Y_sZ_s-axes, as shown in Eq. (63).

$$\frac{Y_s^2}{C_s} + \frac{Z_s^2}{(-C_s/A_s)} = 1. \tag{63}$$

Based on the fact that the image on the screen is represented in the form of Eq. (63), the ellipse radius in the Z_s-axis direction is expressed as $\tan\gamma_\Delta$ as well, where γ_Δ represents the angle bisecting the two tangent lines from the plate element to the ellipse as shown in Fig. 4. The value of $\tan\gamma_\Delta$ is determined by Eq. (64). This equation is derived by evaluating the slope of the tangential lines from the plate element to the ellipse on the xz-plane.

$$\tan\gamma_\Delta = \frac{a^2 - x_0^2 + b^2 - z_0^2}{2\sqrt{-a^2b^2 + a^2z_0^2 + b^2x_0^2}} + \sqrt{\frac{\left(a^2 - x_0^2 + b^2 - z_0^2\right)^2}{4\left(-a^2b^2 + a^2z_0^2 + b^2x_0^2\right)} + 1}. \tag{64}$$

In the $X_sY_sZ_s$ coordinate system, the orientation of the surface is specified as

$$\begin{bmatrix} \cos\gamma_0 & 0 & \sin\gamma_0 \\ 0 & 1 & 0 \\ -\sin\gamma_0 & 0 & \cos\gamma_0 \end{bmatrix} \begin{bmatrix} \cos\theta\cos\varphi \\ \cos\theta\sin\varphi \\ \sin\theta \end{bmatrix}$$

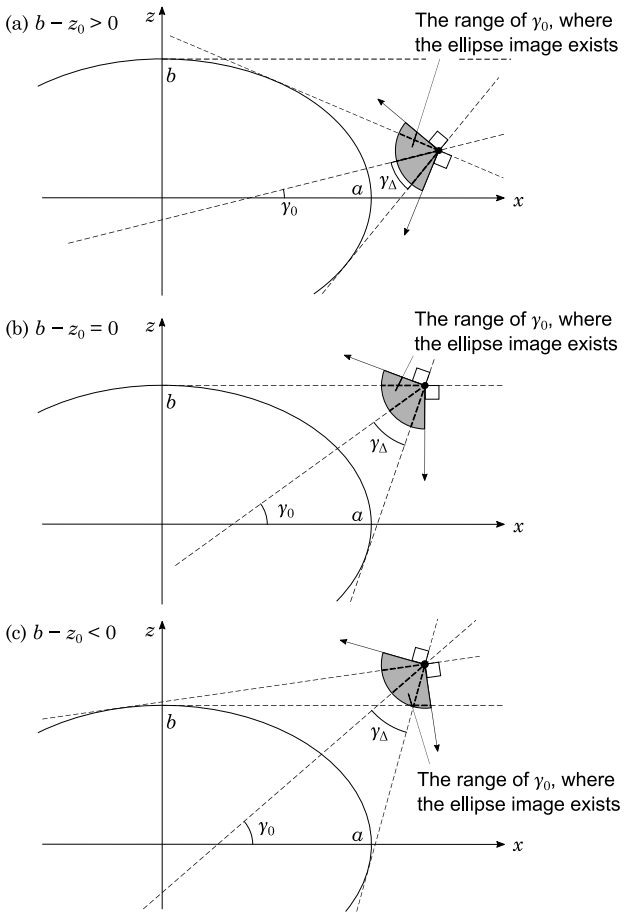

Fig. 4. Range of γ_0 depending on the value of $b - z_0$.

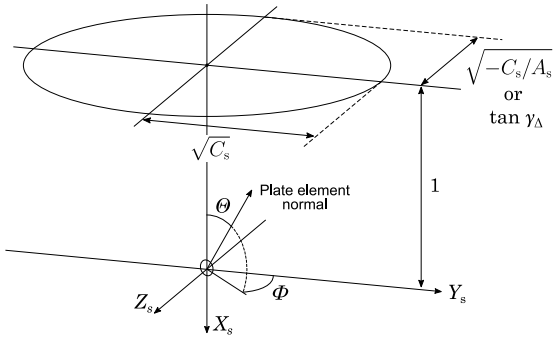

Fig. 5. Ellipse view factor corresponding to the original spheroid view factor.

$$= \begin{bmatrix} \cos\gamma_0\cos\theta\cos\varphi + \sin\gamma_0\sin\theta \\ \cos\theta\sin\varphi \\ -\sin\gamma_0\cos\theta\cos\varphi + \cos\gamma_0\sin\theta \end{bmatrix}. \tag{65}$$

Finally, the original spheroid view factor is equivalent to that of the ellipse shown in Fig. 5. The new angular parameters are

$$\cos\Theta = -\cos\gamma_0\cos\theta\cos\varphi - \sin\gamma_0\sin\theta, \tag{66}$$

$$\tan\Phi = \frac{-\sin\gamma_0\cos\theta\cos\varphi + \cos\gamma_0\sin\theta}{\cos\theta\sin\varphi}. \tag{67}$$

In conclusion, the spheroid view factor from a plate element in arbitrary position and orientation can be calculated as the ellipse view factor.

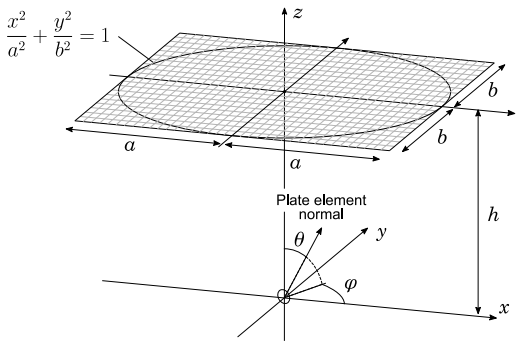

Fig. 6. Numerical evaluation of the ellipse view factor from a plate element.

Table 1
Test parameters for ellipse view factor calculation. The parameter b is specified by $ab = 1$. The total number of test cases is 1710.

Parameter	Values
h	0.1, 1.0, 10.0
a	1.1, 2.0, 10.0
θ [°]	0, 10, 20, ⋯ 180
φ [°]	0, 10, 20, ⋯ 90

4. Numerical validation

In this section, the derived analytical solutions for ellipse and spheroid view factors are validated by numerical calculations. The numerical calculations are performed by summing the view factors of the mesh elements on the ellipse or spheroid surface. In each test, the geometrical parameters are varied, and the differences between the numerical and analytical results are evaluated.

4.1. Ellipse view factor validation

The numerical calculation of the ellipse view factor is performed by integrating the view factor of the rectangular mesh elements. The mesh is generated by dividing the $2a \times 2b$ rectangular area into 4000×4000 sections, as shown in Fig. 6. For each mesh element, which is inside the ellipse, the view factor is calculated based on the basic view factor definition.

$$dF = \frac{\cos\theta_1 \cos\theta_2}{\pi S^2} dA, \tag{68}$$

where

$$S^2 = x^2 + y^2 + h^2, \tag{69}$$

$$\cos\theta_1 = \frac{1}{S}\begin{bmatrix} x \\ y \\ h \end{bmatrix} \cdot \begin{bmatrix} \sin\theta\cos\varphi \\ \sin\theta\sin\varphi \\ \cos\theta \end{bmatrix}, \tag{70}$$

$$\cos\theta_2 = -\frac{1}{S}\begin{bmatrix} x \\ y \\ h \end{bmatrix} \cdot \begin{bmatrix} 0 \\ 0 \\ -1 \end{bmatrix}, \tag{71}$$

$$dA = dxdy. \tag{72}$$

The used parameters for the test cases are summarized in Table 1. The ellipse shape is varied so that the area of the ellipse is constant, determined by $\pi ab = \pi$. For all test cases, the differences between the numerical and analytical results are less than 0.0001. The selected calculation results are shown in Fig. 7.

4.2. Spheroid view factor validation

The numerical calculation of the spheroid view factor is performed by integrating the view factor of the mesh elements on the spheroid surface. The spheroid surface can be presented by the following parametric equation.

$$\begin{bmatrix} x \\ y \\ z \end{bmatrix} = \begin{bmatrix} a\cos\alpha\cos\beta \\ a\cos\alpha\sin\beta \\ b\sin\alpha \end{bmatrix}. \tag{73}$$

where α is the polar angle and β is the azimuthal angle. The differential area of the surface element at (α, β) is described by

$$dA = a\cos\alpha\sqrt{a^2\sin^2\alpha + b^2\cos^2\beta}\; d\alpha d\beta. \tag{74}$$

The normal vector at $(\alpha,\ \beta)$ on the spheroid surface is given by

$$\frac{1}{\sqrt{a^2\sin^2\alpha + b^2\cos^2\alpha}} \begin{bmatrix} b\cos\alpha\cos\beta \\ b\cos\alpha\sin\beta \\ a\sin\alpha \end{bmatrix}. \tag{75}$$

Therefore, the view factor of each mesh element is calculated by Eq. (68), and related variables are specified by

$$S^2 = (x - x_0)^2 + y^2 + (z - z_0)^2, \tag{76}$$

$$\cos\theta_1 = \frac{1}{S}\begin{bmatrix} x - x_0 \\ y \\ z - z_0 \end{bmatrix} \cdot \begin{bmatrix} \cos\theta\cos\varphi \\ \cos\theta\sin\varphi \\ \sin\theta \end{bmatrix}, \tag{77}$$

$$\cos\theta_2 = \frac{1}{S\sqrt{a^2\sin^2\alpha + b^2\cos^2\alpha}} \begin{bmatrix} x_0 - x \\ -y \\ z_0 - z \end{bmatrix} \cdot \begin{bmatrix} b\cos\alpha\cos\beta \\ b\cos\alpha\sin\beta \\ a\sin\alpha \end{bmatrix}. \tag{78}$$

For the validation tests, the spheroid surface is divided into 8000×8000 sections in the polar direction and the azimuthal direction, respectively. The position of the plate element $(x_0, 0, z_0)$ is varied by using the radial parameter r, and the angular parameter ψ, as shown below.

$$x_0 = ra\cos\psi, \tag{79}$$

$$z_0 = rb\sin\psi. \tag{80}$$

Table 2
Test parameters for spheroid view factor calculation. The parameter b is specified by $a^2 b = 1$. The total number of test cases is 43320.

Parameter	Values
a	0.5, 0.9, 1.1, 2.0
r	1.1, 2.0, 10.0
ψ [°]	0, 10, 20, ⋯ 90
θ [°]	−90, −80, ⋯ −10, 0, 10, ⋯ 80, 90
φ [°]	0, 10, 20, ⋯ 180

The used parameters for the validation tests are summarized in Table 2. The spheroid shape is varied so that the volume of the ellipse is constant, determined by $\frac{4}{3}\pi a^2 b = \frac{4}{3}\pi$. For all test cases, the differences between the numerical and analytical results are less than 0.0004. The selected calculation results are shown in Figs. 8 and 9.

5. Conclusion

In this study, the view factors of a spheroid and an ellipse from a plate element are analytically derived. These results are generalization of the analytical view factors of a sphere and circle, and broaden the application possibility in various radiative heat transfer problems. The derived analytical view factors are validated by numerical calculations. In addition to the general derivation method, results of some specific configurations, in which the view factor is described by the simple formula, are presented in Appendix.

CRediT authorship contribution statement

Kaname Sasaki: Conceptualization, Methodology, Software, Writing – original draft, Writing – review & editing, Formal analysis, Validation, Visualization.

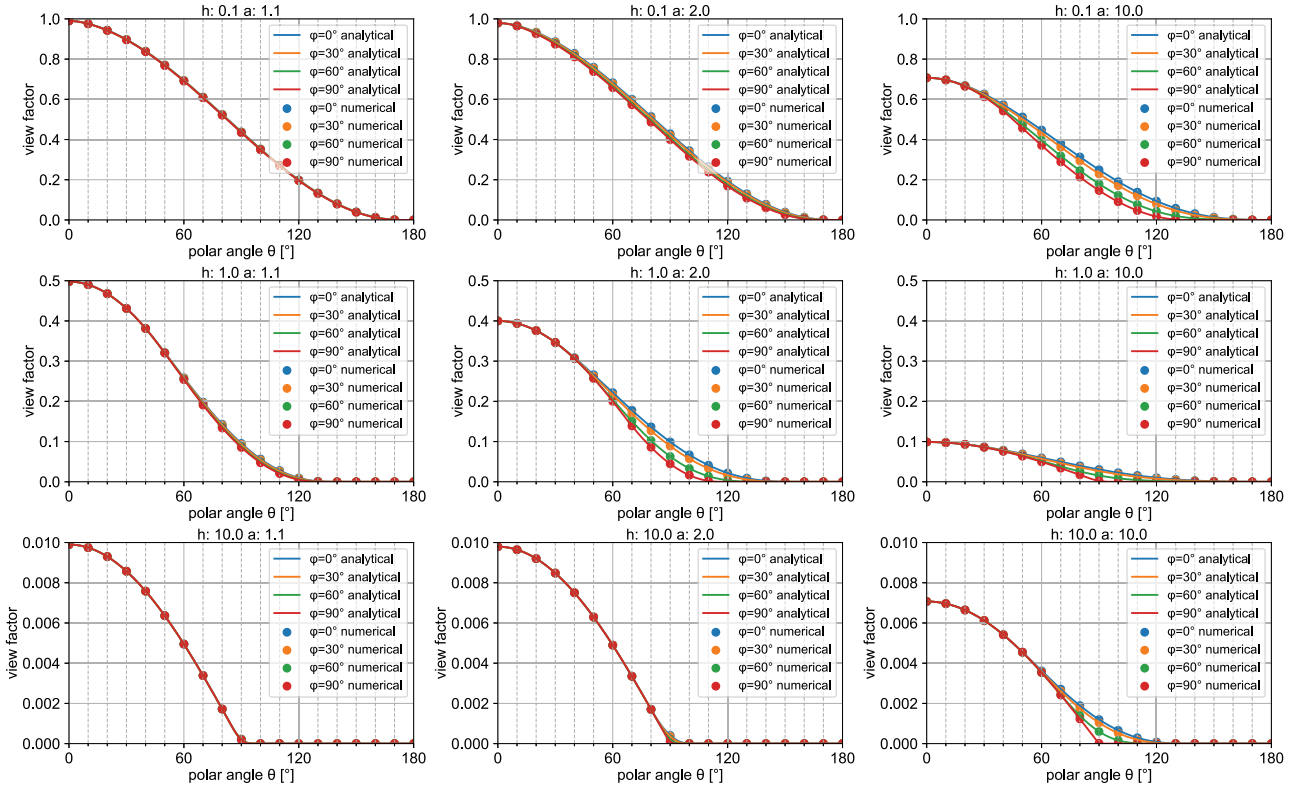

Fig. 7. Selected calculation results from the ellipse view factor verification cases.

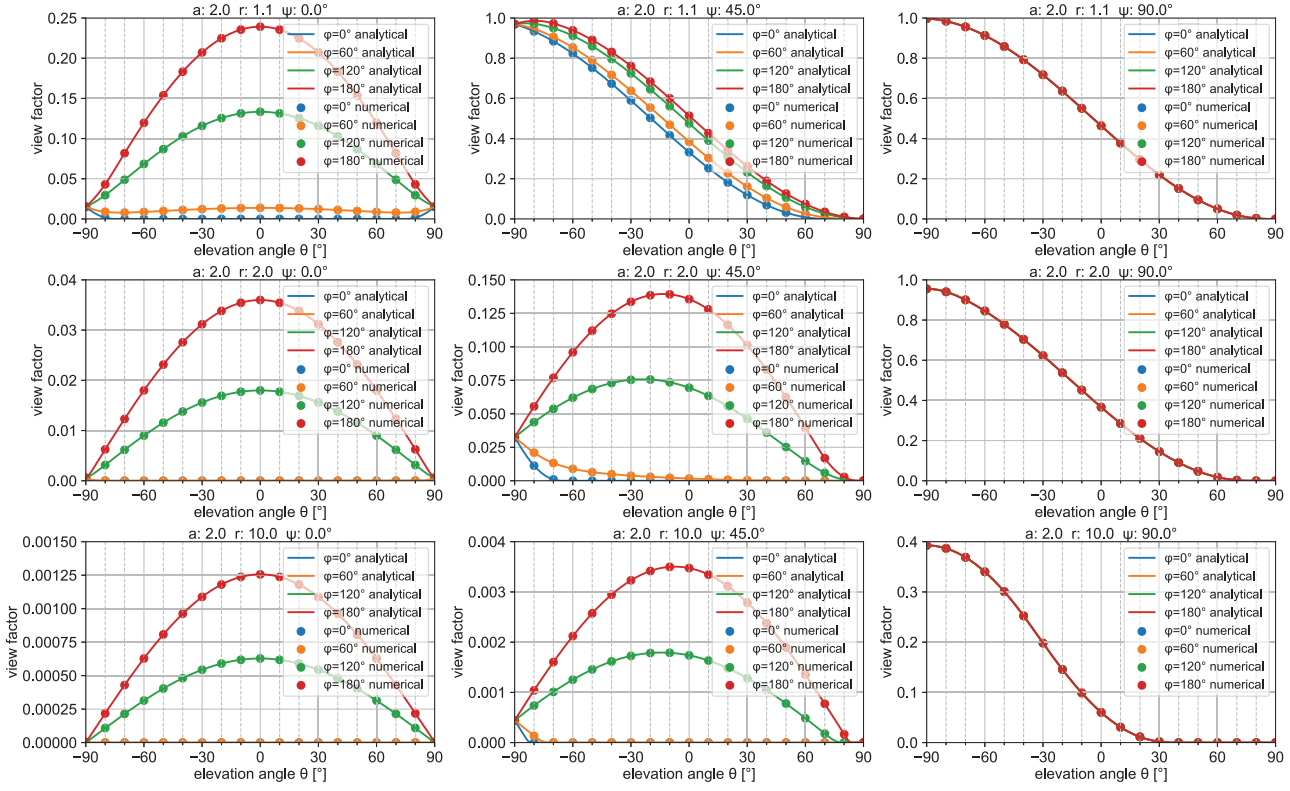

Fig. 8. Selected calculation results from the view factor verification cases for an oblate spheroid.

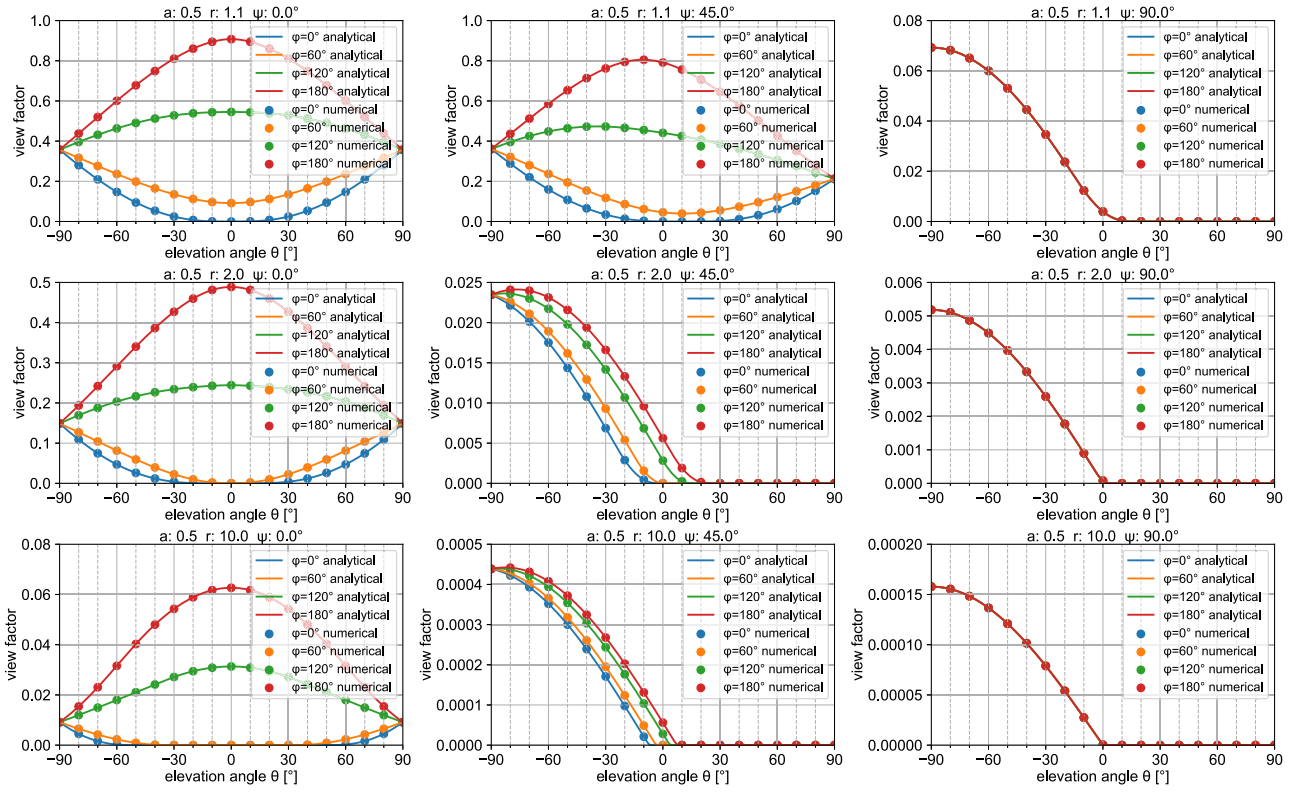

Fig. 9. Selected calculation results from the view factor verification cases for a prolate spheroid.

Declaration of competing interest

The authors declare that they have no known competing financial interests or personal relationships that could have appeared to influence the work reported in this paper.

Data availability

Data will be made available on request.

Appendix. Results for specific configurations

In some specific geometrical configurations, the view factor of an ellipse or a spheroid from a plate element can be expressed in simple formula. In this section, the analytical solutions of such cases are presented.

As discussed in the previous section, the ellipse view factor is calculated by Eq. (18), when the entire ellipse is visible from the plate element. Although the ellipse is not axi-symmetric around the z-axis, the view factor does not depend on the azimuthal angle in this configuration.

When the plate element normal is aligned to the semi-major axis direction as shown in Fig. 10, the view factor is calculated by Eq. (81).

$$F_{\text{Fig.10}} = \frac{-hb}{\pi\sqrt{(a^2-b^2)(a^2+h^2)}}\tanh^{-1}\sqrt{\frac{a^2-b^2}{a^2+h^2}} + \frac{1}{\pi}\arctan\frac{b}{h}. \tag{81}$$

When the plate element normal is aligned to the semi-minor axis direction as shown in Fig. 11, the view factor is calculated by Eq. (82).

$$F_{\text{Fig.11}} = \frac{-ha}{\pi\sqrt{(a^2-b^2)(b^2+h^2)}}\arctan\sqrt{\frac{a^2-b^2}{b^2+h^2}} + \frac{1}{\pi}\arctan\frac{a}{h}. \tag{82}$$

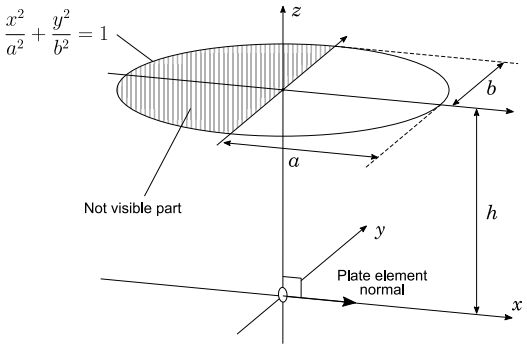

Fig. 10. Ellipse view factor when the plate element is oriented to the semi-major axis (x-axis) direction.

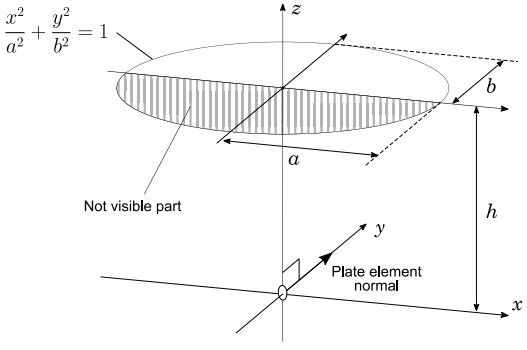

Fig. 11. Ellipse view factor when the plate element is oriented to the semi-minor axis (y-axis) direction.

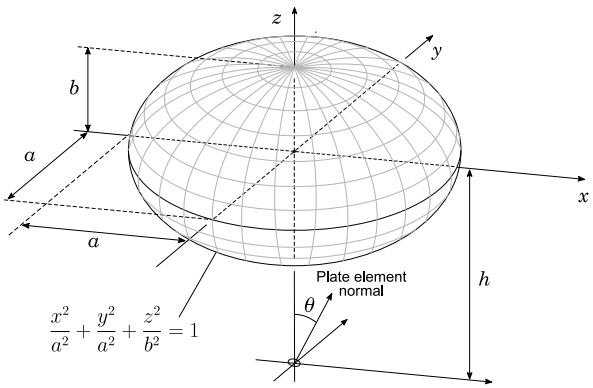

Fig. 12. Spheroid view factor when the plate element is on the z-axis. The extended surface of the plate element does not intersect with the spheroid.

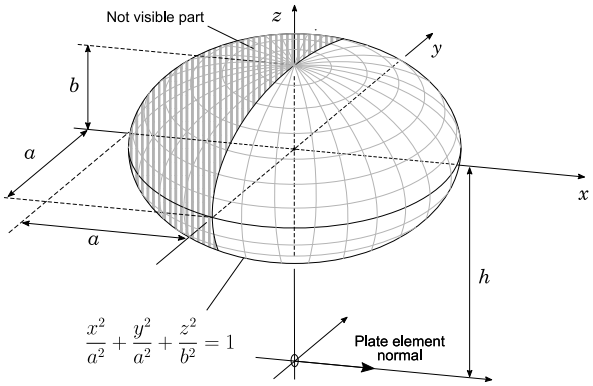

Fig. 13. Spheroid view factor when the plate element is on the z-axis. The surface normal is oriented to the x-axis.

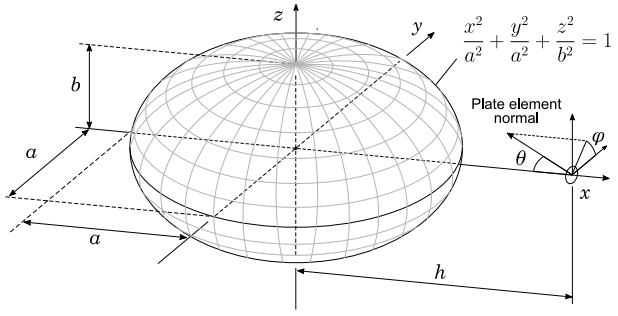

Fig. 14. Spheroid view factor when the plate element is on the x-axis. The extended surface of the plate element does not intersect with the spheroid.

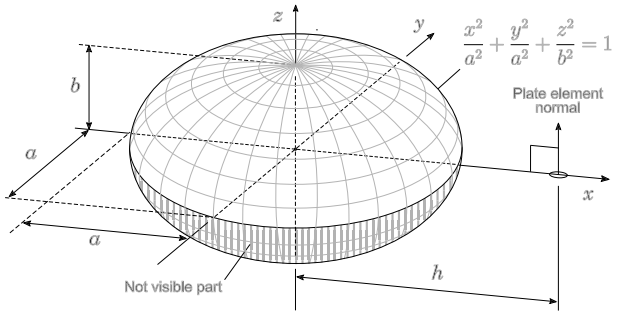

Fig. 15. Spheroid view factor when the plate element is on the x-axis. The surface normal is oriented to the z-axis.

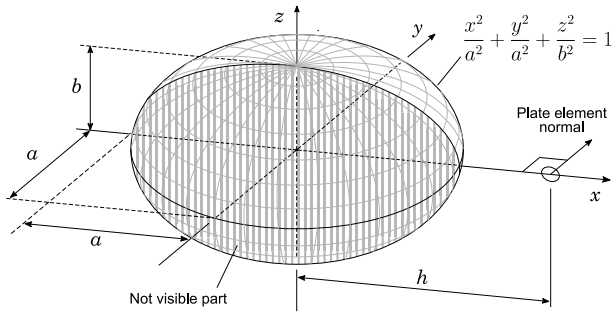

Fig. 16. Spheroid view factor when the plate element is on the x-axis. The surface normal is oriented to the y-axis.

When the plate element is on the z-axis and Eq. (83) is satisfied, the extended plate element surface does not intersect with the spheroid as shown in Fig. 12. In this case, the view factor is independent of the azimuthal orientation of the plate element, and the resulting value is calculated by Eq. (84).

$$\tan^2\theta < \frac{h^2-b^2}{a^2}, \quad \text{and} \quad 0 \le \theta < \frac{\pi}{2}. \tag{83}$$

$$F_{\text{Fig.12}} = \frac{a^2\cos\theta}{a^2+h^2-b^2}. \tag{84}$$

When the plate element is on the z-axis and the orientation is perpendicular to the z-axis as shown in Fig. 13, the view factor is calculated by Eq. (85).

$$F_{\text{Fig.13}} = -\frac{a\sqrt{h^2-b^2}}{\pi(a^2+h^2-b^2)} + \frac{1}{\pi}\arctan\frac{a}{\sqrt{h^2-b^2}}. \tag{85}$$

When the plate element is on the x-axis and Eq. (86) is satisfied, the extended plate element surface does not intersect with the spheroid as shown in Fig. 14. In this case, the view factor is independent of the angular parameter φ, and the resulting value is calculated by Eq. (87).

$$\tan^2\theta < \frac{h^2-a^2}{a^2\cos^2\varphi + b^2\sin^2\varphi}, \quad \text{and} \quad 0 \le \theta < \frac{\pi}{2}. \tag{86}$$

$$F_{\text{Fig.14}} = \frac{ab\cos\theta}{h\sqrt{b^2+h^2-a^2}}. \tag{87}$$

When the plate element is on the x-axis and the plate element normal is aligned to the z-axis as shown in Fig. 15, the analytical expression of the view factor changes depending on whether the spheroid is oblate or prolate. If the spheroid is oblate, where $a > b$, the view factor is calculated by Eq. (88).

$$F_{\text{Fig.15}} = -\frac{a}{\pi}\sqrt{\frac{h^2-a^2}{(a^2-b^2)(b^2+h^2-a^2)}}\arctan\sqrt{\frac{a^2-b^2}{b^2+h^2-a^2}} + \frac{1}{\pi}\arctan\frac{a}{\sqrt{h^2-a^2}}. \tag{88}$$

If the spheroid is prolate, where $a < b$, the view factor is calculated by Eq. (89).

$$F_{\text{Fig.15}} = -\frac{a}{\pi}\sqrt{\frac{h^2-a^2}{(b^2-a^2)(b^2+h^2-a^2)}}\tanh^{-1}\sqrt{\frac{b^2-a^2}{b^2+h^2-a^2}} + \frac{1}{\pi}\arctan\frac{a}{\sqrt{h^2-a^2}}. \tag{89}$$

When the plate element is on the x-axis and the plate element normal is aligned to the y-axis as shown in Fig. 16, the analytical expression of the view factor changes depending on whether the spheroid is oblate or prolate. The view factor of the oblate spheroid is calculated by Eq. (90).

$$F_{\text{Fig.16}} = -\frac{b}{\pi h}\sqrt{\frac{h^2-a^2}{a^2-b^2}}\tanh^{-1}\frac{\sqrt{a^2-b^2}}{h}$$

$$+ \frac{1}{\pi} \arctan \frac{b}{\sqrt{h^2 - a^2}}. \tag{90}$$

The view factor of the prolate spheroid is calculated by Eq. (91).

$$F_{\text{Fig.16}} = -\frac{b}{\pi h} \sqrt{\frac{h^2 - a^2}{b^2 - a^2}} \arctan \frac{\sqrt{b^2 - a^2}}{h} + \frac{1}{\pi} \arctan \frac{b}{\sqrt{h^2 - a^2}}. \tag{91}$$

References

[1] Howell JR, Mengüç MP. Radiative transfer configuration factor catalog: A listing of relations for common geometries. J Quant Spectrosc Radiat Transfer 2011;112(5):910–2.

[2] Howell JR. A catalogue of radiation heat transfer configuration factors, 3rd edition. https://www.thermalradiation.net/indexCat.html.

[3] Chung BTF, Naraghi MHN. Some exact solutions for radiation view factors from spheres. AIAA J 1981;19(8):1077–81.

[4] Chung BTF, Naraghi MHN. A simpler formulation for radiative view factors from spheres to a class of axisymmetric bodies. J Heat Transfer 1982;104(1):201–4.

[5] Sabet M, Chung BTF. Radiation view factors from a sphere to nonintersecting planar surfaces. J Thermophys Heat Transfer 1988;2(3):286–8.

[6] N Naraghi MH. Radiative view factors from spherical segments to planar surfaces. J Thermophys Heat Transfer 1988;2(4):373–5.

[7] Sasaki K, Sznajder M. Analytical view factor solutions of a spherical cap from an infinitesimal surface. Int J Heat Mass Transfer 2020;163:120477.

[8] Naraghi MHN, Chung BTF. Radiation configuration factors between disks and a class of axisymmetric bodies. J Heat Transfer 1982;104(3):426–31.

[9] Cabeza-Lainez JM, Pulido-Arcas JA. New configuration factors for curved surfaces. J Quant Spectrosc Radiat Transfer 2013;117:71–80.

[10] Blankenhagel P, Wehrstedt K-D, Mishra KB, Steinbach J. Thermal radiation assessment of fireballs using infrared camera. J Loss Prev Process Ind 2018;54:246–53.

[11] Hankinson G, Lowesmith BJ. A consideration of methods of determining the radiative characteristics of jet fires. Combust Flame 2012;159(3):1165–77.

[12] Zhou K, Liu J, Jiang J. Prediction of radiant heat flux from horizontal propane jet fire. Appl Therm Eng 2016;106:634–9.

[13] Zhou K, Jiang J. Thermal radiation from vertical turbulent jet flame: Line source model. J Heat Transfer 2016;138(4).

[14] Aziz NSA, Kasmani RM, Samsudin MDM, Ahmad A. Comparative analysis on semi-empirical models of jet fire for radiant heat estimation. Process Integr Optim Sustain 2019;3:285–305.

[15] Xu L, Lu Y, Ding C, Guo H, Liu J, Zhao Y. A generic flame shape model and analytical models for geometric view factor calculation on the fire exposure surface. Int J Therm Sci 2022;173:107392.

[16] Markan A, Baum HR, Sunderland PB, Quintiere JG, de Ris JL. Transient ellipsoidal combustion model for a porous burner in microgravity. Combust Flame 2020;212:93–106.

[17] Dehghani P, Sunderland PB, Quintiere JG, deRis JL. Burning in microgravity: Experimental results and analysis. Combust Flame 2021;228:315–30.

[18] Dehghani P, Quintiere JG. Theoretical analysis and predictions of burning in microgravity using a burning emulator. Combust Flame 2021;233:111572.

[19] Colaizzi PD, Evett SR, Howell TA, Li F, Kustas WP, Anderson MC. Radiation model for row crops: I. Geometric view factors and parameter optimization. Agron J 2012;104(2):225–40.

[20] Colaizzi PD, Schwartz RC, Evett SR, Howell TA, Gowda PH, Tolk JA. Radiation model for row crops: II. Model evaluation. Agron J 2012;104(2):241–55.

[21] Zhang K, Zhang T, Spence C, Qi F. A new method for calculating the view factor from a wall to a spheroidal canopy. Build Environ 2023;241:110419.

[22] Lu T, Lin X, Lan W. On the calculation method of the view factor for earth to aerostats. In: 2016 35th Chinese control conference. 2016, p. 2011–5. http://dx.doi.org/10.1109/ChiCC.2016.7553661.

[23] Hongpeng N, Xianwu L, Zhibin L, Weiyao L. A 3-parameter thermal model for the skin of stratospheric airships and its computing analysis. In: 2017 36th Chinese control conference. 2017, p. 2082–7. http://dx.doi.org/10.23919/ChiCC.2017.8027662.

[24] Pelivan I, Drube L, Kührt E, Helbert J, Biele J, Maibaum M, et al. Thermophysical modeling of Didymos' moon for the Asteroid Impact Mission. Adv Space Res 2017;59(7):1936–49.

[25] Togno SD, Brouquet H, Messina G. Implementation of temperature dependant thermo-optical properties and complex 3D geometry using ESATAN-TMS. In: 40th international conference on environmental systems. 2010, http://dx.doi.org/10.2514/6.2010-6115.

[26] Naraghi MHN. Radiation view factors from differential plane sources to disks - A general formulation. J Thermophys Heat Transfer 1988;2(3):271–4.

[27] Cabeza-Lainez JM, Pulido-Arcas JA, Sanchez-Montañés B, Rubio-Bellido C. New configuration factor between a circle and a point-plane at random positions. Int J Heat Mass Transfer 2014;69:147–50.

[28] Wong H. Heat transfer for engineers. Longman Group Limited; 1977.

[29] Siegel R, Howell JR. Thermal radiation heat transfer. 3rd ed. Hemisphere Publishing Corporation; 1992.

[30] Sparrow EM. A new and simpler formulation for radiative angle factors. J Heat Transfer 1963;85(2):81–7.

[31] Wokes DS. Autonomous pose estimation of a passive target [Ph.D. thesis], University of Surrey; 2010.

[32] Wokes DS, Palmer PL. Perspective reconstruction of a spheroid from an image plane ellipse. Int J Comput Vis 2010;90:369–79.